Clinical Neurophysiology 153 (2023) 88–101

Contents lists available at ScienceDirect

Clinical Neurophysiology

journal homepage: www.elsevier.com/locate/clinph

Electromagnetic source imaging predicts surgical outcome in children with focal cortical dysplasia

Rupesh Kumar Chikara [a,b], Saeed Jahromi [a,b], Eleonora Tamilia [c], Joseph R. Madsen [d], Steve M. Stufflebeam [e], Phillip L. Pearl [f], Christos Papadelis [a,b,g,*]

[a] Jane and John Justin Institute for Mind Health, Neuroscience Research, Cook Children's Health Care System, Fort Worth, TX, USA
[b] Department of Bioengineering, University of Texas at Arlington, Arlington, TX, USA
[c] Fetal-Neonatal Neuroimaging and Developmental Science Center, Boston Children's Hospital, Harvard Medical School, Boston, MA, USA
[d] Division of Epilepsy Surgery, Department of Neurosurgery, Boston Children's Hospital, Harvard Medical School, Boston, MA, USA
[e] Athinoula Martinos Center for Biomedical Imaging, Massachusetts General Hospital, Harvard Medical School, Boston, MA, USA
[f] Division of Epilepsy and Clinical Neurophysiology, Department of Neurology, Boston Children's Hospital, Harvard Medical School, Boston, MA, USA
[g] School of Medicine, Texas Christian University, Fort Worth, TX, USA

HIGHLIGHTS

- Epileptic foci are localized more accurately with electromagnetic source imaging compared to individual modalities.
- Electromagnetic source imaging predicts surgical outcome better than individual modalities.
- Electromagnetic source imaging offers higher localization accuracy than individual modalities.

ARTICLE INFO

Article history:
Accepted 15 June 2023
Available online 5 July 2023

Keywords:
Electromagnetic source imaging
Epilepsy surgery
Focal cortical dysplasia
Intracranial EEG
Irritative zone
Seizure onset zone

ABSTRACT

Objective: To evaluate the diagnostic accuracy of electromagnetic source imaging (EMSI) in localizing spikes and predict surgical outcome in children with drug resistant epilepsy (DRE) due to focal cortical dysplasia (FCD).
Methods: We retrospectively analyzed magnetoencephalography (MEG) and high-density (HD-EEG) data from 23 children with FCD-associated DRE who underwent intracranial EEG and surgery. We localized spikes using equivalent current dipole (ECD) fitting, dipole clustering, and dynamical statistical parametric mapping (dSPM) on EMSI, electric source imaging (ESI), and magnetic source imaging (MSI). We calculated the distance from the seizure onset zone (D_{SOZ}) and resection (D_{RES}). We estimated receiver operating characteristic (ROC) curves with Youden's index (J) to predict outcome.
Results: EMSI presented shorter D_{SOZ} (15.18 ± 9.06 mm) and D_{RES} (8.56 ± 6.24 mm) compared to ESI (D_{SOZ}: 25.04 ± 16.20 mm, $p < 0.009$; D_{RES}: 18.88 ± 17.30 mm, $p < 0.03$) and MSI (D_{SOZ}: 23.37 ± 8.98 mm, $p < 0.03$; D_{RES}: 15.51 ± 10.11 mm, $p < 0.02$) for clustering in patients with good outcome. Clustering showed shorter D_{SOZ} and D_{RES} compared to ECD fitting and dSPM ($p < 0.05$). EMSI had higher performance as outcome predictor (J = 70.63%) compared to ESI (J = 41.27%) and MSI (J = 33.33%) for clustering.
Conclusions: EMSI provides superior localization and improved predictive performance than individual modalities.
Significance: EMSI can help the surgical planning and facilitate the localization of epileptogenic foci.

1. Introduction

Focal cortical dysplasia (FCD) represents the most common structural brain lesion in children with drug resistance epilepsy (DRE) (Kabat and Król, 2012; Knight et al., 2015). Surgical resection (or laser ablation) of this lesion can lead to seizure freedom or to a significant decrease in the number of seizures (Dallas et al., 2020; Kwan and Brodie, 2000). Magnetic resonance imaging (MRI) plays critical role in the non-invasive identification of the lesion. Yet, it fails to localize up to 87% of FCD 1 and 33% of FCD 2 lesions (Pittau et al., 2017; Tassi et al, 2012), and to delineate their exact boundaries. Furthermore, the lesion does not always coincide with

* Corresponding author at: Jane and John Justin Institute for Mind Health, Neuroscience Research, Cook Children's Health Care System, 1500 Cooper St., Fort Worth, TX 76104, USA.
E-mail address: christos.papadelis@cookchildrens.org (C. Papadelis).

https://doi.org/10.1016/j.clinph.2023.06.015
1388-2457/

the epileptogenic zone (EZ), the brain area that is indispensable for the generation of seizures, which should be resected (or ablated) in order the patient to become seizure free. Thus, a comprehensive presurgical evaluation is often required that includes several non-invasive electrophysiological tests, such as high-density electroencephalography (HD-EEG) and magnetoencephalography (MEG) (Rosenow and Lüders, 2001).

Through electric and magnetic source imaging (ESI/MSI), HD-EEG and MEG allow the non-invasive localization of the irritative zone, the brain area that generates interictal epileptiform discharges (IEDs). Previous studies have explored the contribution of ESI and MSI in the presurgical evaluation of patients with DRE (Tamilia et al., 2019; Sharma et al., 2019; Foged et al., 2020). By comparing their localization findings with those from intracranial EEG (iEEG), these studies found that ESI and MSI could localize the irritative zone with an accuracy ranging from ~15 to 19 mm for ESI (Birot et al., 2014, Mégevand et al., 2014, Tamilia et al., 2019, Ntolkeras et al., 2022), and ~9 to 15 mm for MSI (Kim et al., 2016, Tamilia et al., 2019, Ntolkeras et al., 2022). Few studies extended these findings by assessing the clinical utility of ESI and MSI in epilepsy surgery through estimating predictive values of surgical outcome (ESI: Kaur et al., 2021; Stefan et al., 2003; Pataraia et al., 2004; Paulini et al., 2007; MSI: Kaur et al., 2021; Stefan et al., 2003; Pataraia et al., 2004; Paulini et al., 2007). These studies found that ESI revealed the EZ with a localization accuracy ranging from 57 to 61%, sensitivity from 60 to 63%, and specificity from 47 to 63% (Baroumand et al. 2018; Sharma et al., 2018). MSI showed a localization accuracy ranging from 58 to 74%, sensitivity from 79 to 82%, and specificity from 38 to 53% (Kaur et al., 2021; Mouthaan et al., 2019; Stefan et al., 2003; Pataraia et al., 2004). Other studies also found that MSI led to a change in the clinical decision-making plan in 21 to 33% of patients with DRE (Knowlton et al. 2009; De Tiege et al. 2012). Only few studies have assessed the clinical utility of ESI/MSI for patients with FCD-associated DRE reporting a localization accuracy ranging from 50 to 66% for ESI (Bast et al., 2004; Hauptman and Mathern, 2012) and 45% for MSI (Bast et al., 2004), respectively. Thus, ESI and MSI are useful presurgical tools that contribute to the noninvasive delineation of the irritative zone in patients with DRE.

Despite these evidences, ESI and MSI are currently performed in only few tertiary epilepsy centers on a regular basis. Moreover, HD-EEG and MEG are rarely recorded simultaneously in spite of the fact that they yield both confirmatory and complementary information and present several limitations when they are used on their own. MSI has higher spatial resolution than ESI (Singh, 2014; Hari et al., 2018; Tamilia et al., 2019), but is almost blind to epileptiform activity originated from deep brain structures (Singh, 2014; Hari et al., 2018), such as the hippocampus or amygdala, or sources having radial orientation (i.e., gyral crest depolarization) (Stapleton et al., 2018; Hari et al., 2018). On the other hand, ESI can detect activity from both radially and tangentially oriented sources (Baillet, et al., 1999, Cohen and Cuffin, 1987, Fuchs, et al., 1998, Liu, et al., 2002, Wolters, et al., 2006) as well as from sources located in subcortical brain regions (Seeber et al., 2019). Therefore, approximately 30% of the epileptiform activity is visible in only one modality (Stapleton et al., 2018; Hari et al., 2018; Heers, et al., 2010; Knowlton et al., 2009; Knake at al., 2006). Moreover, the ESI is sensitive to the geometry and conductivity of skull, while the MSI is not affected by the skull's conductivity (Hamalainen, et al., 1993, Wolters, et al., 2006). Finally, ESI is more susceptive to artifacts compared to MSI (Hari et al., 2018; Stefan et al., 2003; Knake at al., 2006; Papadelis et al., 2016).

Former theoretical, modeling, and stimulation studies as well as empirical data suggest that the combination of these two techniques into a single solution, namely electromagnetic source imaging (EMSI), would provide more accurate localization compared to the individual solutions (Cuffin and Cohen, 1979; Cohen and Cuffin, 1983; Fuchs et al., 1998; Wood et al., 1982; Baumgartner et al., 2000). By comparing the localization of visual evoked neural activity obtained with MEG and HD-EEG with the foci of functional magnetic resonance imaging (fMRI) activation produced by identical stimuli, Sharon and colleagues (Sharon et al., 2007) showed that the localization results of EMSI are superior to those obtained by either modality alone. In a case series of patients with DRE undergone surgery, Yoshinaga and colleagues (Yoshinaga et al., 2002) showed that the EMSI analysis provided information that would not have been obtained by the use of either modality individually, and in one of these patients combined use led to successful localization for surgery. Later, Pataraia and colleagues (Pataraia et al., 2005) showed that EMSI can identify sub-compartments of the temporal lobe involved in epileptic activity and may be helpful in differentiating between subtypes of mesial temporal lobe epilepsy. More recently, a prospective blinded study in a cohort of 30 patients with DRE found that EMSI achieved higher odds ratio compared to individual modalities, and thus provided clinically useful, new information in 34% of the cases (Duez et al., 2019). Despite this converging evidence, ESI and MSI are rarely explicitly combined for the localization of the irritative zone possibly due to lack of research in the field reinforcing its use in the presurgical evaluation of patients with DRE.

The main aim of our study is to quantify and compare the accuracy of ESI, MSI, and EMSI in localizing IEDs prior to surgery in children with FCD, and to assess the utility of EMSI against the gold standard of seizure freedom after resection. We hypothesize that EMSI provides critical additive information compared to individual modalities (i.e., ESI and MSI) in the presurgical evaluation of patients with FCD-associated DRE. To pursue our aim and test our hypothesis, we localized IEDs occurred in both MEG (204 gradiometers and 102 magnetometers) and HD-EEG (72 electrodes) recordings with ESI, MSI, and EMSI using dipole fitting with clustering and a distributed source localization method (i.e., dynamic Statistical Parametric Mapping – dSPM). We then defined the ground-truth irritative zone at the source level using ESI performed on iEEG recordings (i.e., ESI-iEEG). We measured and compared the distance of the inverse solutions for the three modalities (i.e., ESI, MSI, and EMSI) from the clinically defined seizure onset zone (D_{soz}) and resection (D_{RES}). We finally estimated receiver operating characteristic curves (ROCs) to assess the performance of each modality in predicting surgical outcome.

2. Methods

2.1. Patients

From June 2011 to July 2017, we retrospectively reviewed pediatric patients with DRE who underwent epilepsy surgery at Boston Children's Hospital (BCH). The following criteria were used to determine which patients would be included in the study: (i) histological confirmation of FCD; (ii) long-term monitoring with iEEG (using grids, strips, or sEEG depth electrodes); (iii) availability of pre-surgical MRI, post-implantation computerized tomography (CT), and post-operative MRI; and (iv) at least one year of post-surgical follow up. Our institutional review board approved the study protocol. Due to the retrospective nature of the study, written informed consents were not required. As part of our institution's clinical practice, the histological confirmation of FCD was performed using microscopic analysis of the removed tissue. All samples were categorized using the new FCD classification scheme developed by the International League against Epilepsy (ILAE) (Blümcke et al., 2011).

2.2. Simultaneous HD-EEG and MEG recordings

Simultaneous MEG and HD-EEG recordings were carried out at the MEG Core Laboratory of Athinoula Martinos Center for Biomedical Imaging (Charlestown, MA). The followed procedures were according to Hari and colleagues (Hari et al., 2018). MEG recordings were performed by using a whole head 306 sensor system (VectorView, Elekta Neuromag, Helsinki, Finland), which includes 204 planar gradiometers and 102 magnetometers placed at 102 locations. The MEG system was located inside a three-layer magnetically shielded room (Imedco, Hägendorf, Switzerland). Using a non-magnetic 70-channels electrode cap (EASYCAP, Herrsching, Germany), simultaneous HD-EEG data were captured. The EEG electrodes were positioned according to the 10–10 system. Two additional EEG electrodes were placed in temporal areas (i.e., T1 / T2). The reference electrode was placed at the tip of the patient's nose (Hari et al., 2017). Four Head Position Indicator (HPI) coils were placed on the patient's head. A three-dimensional (3D) digitizer was used to measure the positions of HPI coils and EEG electrodes in relation to anatomical markers on the patient's skull. This made it possible to align the coordinate systems of MEG, HD-EEG, and MRI. Additional electrodes were also placed to estimate horizontal and vertical electrooculography (EOG) and electrocardiography (ECG). All recordings were completed in the supine position. The patients were instructed to relax (or sleep) during the recordings. The data collection was performed with a sampling rate of 1 KHz and an online low-pass Infinite Impulse Response (IIR) filter of sixth order at 400 Hz. The signals were collected in different sessions (10 to 12 sessions per patient lasting 4 to 5 minutes each). Before the start of each session, the head position was measured by activating the HPI coils. More information about the protocol is provided in our former studies (Papadelis et al., 2016; Tamilia et al., 2019).

2.3. iEEG recordings

Following consensus of the multidisciplinary epilepsy surgery conference at BCH, iEEG recordings were carried out for all patients (Tamilia et al., 2019). The aim of iEEG implantation was to monitor all potential epileptogenic regions that considered "of interest" based on a comprehensive presurgical evaluation of patient's medical record. The iEEG implantation was independent of this investigation. The multidisciplinary clinical team reached a conclusion about the iEEG electrodes implantation and/or the margins of surgical resection based on semiology, FDG-PET, ictal SPECT, MRI, and interictal MSI findings. The HD-EEG data presented in this study were not considered in the patients' presurgical evaluation. The MSI findings, which were considered in the clinical decision about the margins of cortical resection, were based on ECD analysis that was performed by a different reader (than the one performed the analysis for this study) using a different data analysis software (i.e., Elekta-NeuromagXfit).

The iEEG recordings were performed through subdural grids and strips (2.3 mm exposure diameter, 10 mm distance) and/or depth electrodes (10 contacts placed linearly: 1.1 mm in diameter, 3–5 mm between spacing; Ad-Tech., USA). The recordings were performed with a sampling rate ranging from 500 to 2,048 Hz using the XLTEK NeuroWorks system (Natus Inc., USA). According to the clinical practice at BCH, the original reference for the subdural grids or strips was a four-contact strip facing the dura. For the iEEG recordings performed with depth electrodes, the original reference was in the white matter.

2.4. MRI and CT acquisition

Using a high-resolution 3 T scanner (TIM TRIO, Siemens AG, Erlangen, Germany), MRI was obtained before and after surgical resection with magnetization-prepared rapid acquisition gradient-echo sequences (MPRAGE; TE = 1.74 ms, TR = 2, 520 ms, voxel size = 111 mm), according to a protocol that has been detailed in prior studies (Prabhu et al., 2015). After iEEG implantation, a CT scan (voxel size = 0.5 × 0.5 × 0.5 mm) was performed to confirm the accurate placement of iEEG electrodes. The anatomical location of each iEEG contact was identified for each patient through coregistering the presurgical MRI and post-implantation CT. The coordinate of each contact was initially determined manually through visual inspection of the co-registered CT-MRI image and projecting on patient's cortical surface 3D model that was created from their preoperative MRI using *FreeSurfer* (Dale et al., 1999). To avoid the brain's shift problem resolution, we used an in-house algorithm developed by our group in Matlab 2019a (The MathWorks, Inc.) (Matarrese et al., 2021).

2.5. Clinically defined SOZ

The SOZ was clinically defined independently from this study. The location of all iEEG contacts where the earliest change in background activity related to each captured clinical seizure (SOZ contacts) was identified by a pediatric epileptologist. All contacts identified as part of the SOZ were used to define the SOZ for each patient.

2.6. Selection of interictal data for HD-EEG, MEG, and iEEG

HD-EEG, MEG, and iEEG marking of interictal events was performed independently of surgical planning. HD-EEG and iEEG recordings were examined in both bipolar and average reference montages. Two independent readers (E. Tamilia and C. Papadelis), who were blind to each other's markings, identified segments containing interictal activity in the HD-EEG, MEG, and iEEG recordings. These readers were not part of the multidisciplinary team that decided the patient's surgical planning. Furthermore, they were unaware of the clinical history and outcomes of the patients during the marking of interictal events. In case of disagreement, a more experienced reviewer (P.L. Pearl), who was blinded to patient's outcome, reviewed the questionable activity.

2.7. Identification of IEDs

Channels with persistent artifacts (or noise) were excluded from all modalities. The IEDs were identified in filtered data (band-pass filter: 1–70 Hz; notch filter: 60 Hz and harmonics) through visual inspection by two independent readers (E. Tamilia and C. Papadelis), who did not see the marking of others or the history of each patient. The IEDs marking was performed independently for each modality according to the following criteria (Chatrian, 1974): (i) paroxysmal occurrence; (ii) abrupt change in polarity; (iii) consistent topography of the scalp with a physiological field; and (iv) duration < 200 ms. For the visual identification of IEDs, an average montage was applied to the iEEG, whereas both average and bipolar montages were applied to the HD-EEG. For MEG, the Signal Space Projection (SSP) analysis was used to reject external disturbances caused by cardiac events identified by ECG. The signals of the 306 sensors were displayed in groups of 38–39 each covering a specific brain region (i.e., left and right frontal, left and right temporal, left and right parietal, and left and right occipital). The IEDs marking was performed on a region-by-region basis. Similarly, for iEEG, channels from the same strip, grid, or depth electrode were examined together. For all modalities, IEDs were initially marked at the peak of spikes in *Brainstorm* (Tadel et al., 2011).

Considering that IEDs do not always occur at the same exact time in MEG and HD-EEG signals (see Results section), we analyzed

further only IEDs having a temporal distance of < 30 ms between the two modalities (i.e., latency between the spike peaks on MEG and HD-EEG signals) (Fig. 1a). For each of these events, EMSI was performed at the mid-point between the spike peaks occurred in MEG and EEG signals. We followed this approach in order to avoid a bias of source localization findings towards a specific modality. For the EMSI, we used the inbuilt algorithms in Brainstorm, which have been described in detail previously (Baillet et al., 1999; Tadel et al., 2011; 2019). ESI and MSI were performed at the peak of IEDs, which were identified at the HD-EEG and MEG signals, respectively.

2.8. Source localization of IEDs

2.8.1. Forward model

Using the *OpenMEEG* software, we created a realistic head model from each patient's MRI (Fig. 1b) (Gramfort et al., 2010). Utilizing *Freesurfer* with the default parameter settings, the individual cortical surfaces were extracted from each patient's MRI volume (Tadel et al., 2011). For HD-EEG and MEG signals analysis, the realistic boundary elementary model (BEM) was created using a three-layer consisting of the scalp, outer skull, and inner skull. For iEEG analysis, we used a one-layer (inner skull) BEM model. The adaptive integration method in Brainstorm (Dale et al., 1999) was used to create a grid of points that sampled the entire brain volume to also considering the deeper or subcortical brain regions.

2.8.2. Equivalent current dipoles (ECDs)

The source of each IED was localized with the ECD model (Knowlton et al. 1997; Stefan et al. 2003). Using a dipole scanning technique supported by *Brainstorm*, unconstrained source analysis was carried out in the volume space (Tadel et al., 2011). This method identifies the most significant dipole in a 3D dipoles grid which are already estimated. The grid is reconstructed from the entire brain volume of each patient's MRI (5 mm spatial resolution). In order to prevent merging IEDs that came from several sources, we opted to localize each IED individually rather than on averaged signal (Diekmann et al., 1998; Tamilia et al., 2019). Fig. 1c shows an example of ECDs findings for all modalities (i.e., ESI, MSI, EMSI, and ESI-iEEG) in a 17-year-old female with FCD from our cohort (patient #10, Table 1). Only ECDs of all modalities with a Goodness of Fit (GOF) greater than 60% were taken into consideration (Alhilani et al., 2020; Tamilia et al., 2020).

2.8.3. Clustering

Clustering analysis was performed for ECDs of all modalities (i.e., ESI, MSI, EMSI, and ESI-iEEG) (Ntolkeras et al., 2022). We measured the number of dipoles that are clustered around it within a 15 mm radius distance. Then, we normalize this measurement by

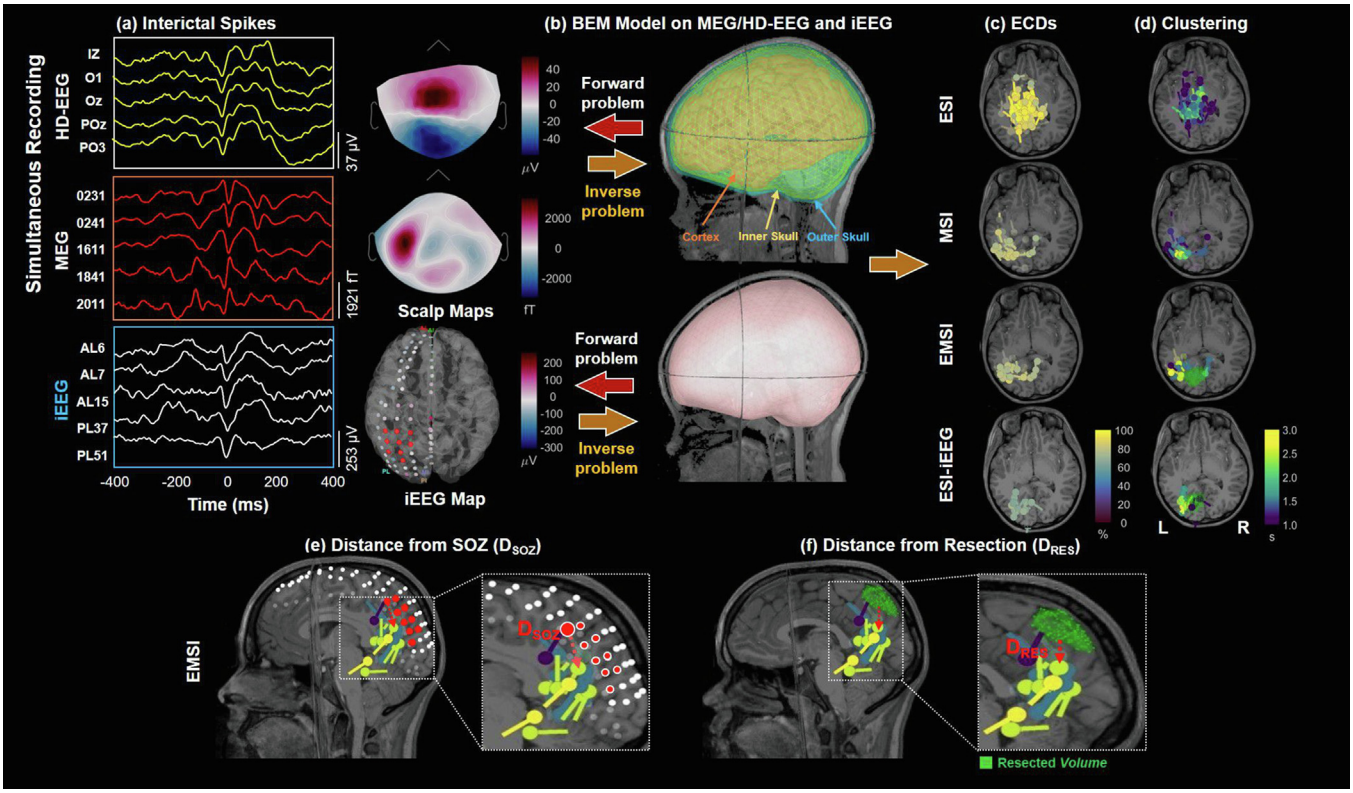

Fig. 1. Interictal epileptiform discharges (IEDs) on combined electromagnetic source imaging (EMSI) and intracranial electroencephalography (iEEG) data. (a) Example of concurrent IED on simultaneous HD-EEG and MEG recordings, and iEEG recordings from a patient with DRE. Data from patient #10 (17-year-old female with DRE, resected lobe left parietal, good outcome). Simultaneous HD-EEG and MEG recordings, and iEEG data from −400 to 400 ms around IED filtered between 1–70 Hz. Topographic maps of the electrical potential and magnetic field are perpendicular between HD-EEG and MEG signals. Polarity changes for both the non-invasive (i.e. MEG and HD-EEG) and invasive (iEEG) recordings indicate an underlying focal dipolar source in left parietal region. (b) The boundary elementary model (BEM) was created using a three-layer consisting of the scalp, outer skull, and inner skull on combined HD-EEG + MEG. For iEEG, we used a one-layer (inner skull) BEM model. (c) Equivalent current dipoles (ECDs) are shown in HD-EEG, MEG and combined HD-EEG + MEG modalities for the same patient. (d) Clustering are revealed in HD-EEG, MEG and combined HD-EEG + MEG modalities (dipole clusterness represented via yellow). (e&f) Estimation of distance from the SOZ (D_{SOZ}) and distance from resection (D_{RES}). Distance of each within-coverage dipole from the SOZ (D_{SOZ}) is calculated as its Euclidian distance from the closest SOZ contact (red arrow). Distance of each dipole from the resection cavity is defined by the Euclidean distance of each dipole from the closest points of the resected volume (D_{RES}, red arrow). The resected volume (green volume) is defined by marking the volume points corresponding to the resection cavity on the postsurgical MRI coregistered with the presurgical MRI. Note: iEEG recordings were not performed simultaneously with MEG and HD-EEG. DRE = drug resistant epilepsy; SOZ = seizure onset zone.

dividing it with the total number of dipoles for this patient (range: 0–100%) (Fig. 1d). This normalized measurement is known as the "clusterness" of the dipole. The 15 mm distance cut-off is based on previous studies indicating that this distance corresponds to the width of a gyrus (Ono et al., 1990). This suggests that, even if they are not always in the same gyrus, the ECDs are close to each other within a gyral width (Kim et al., 2016).

2.8.4. Dynamical statistical parametric mapping (dSPM)

Each IED was also localized with a distributed source modelling method, namely dSPM (Dale et al., 2000). The dSPM assumes that all EEG (or MEG) activity is produced by extended sources in the brain volume. For each modality, we measured the location of the underlying sources at the peak of each IED (volume points that show > 90% of the maximum dSPM value). Then, for each patient, the sources of all IEDs merged into a single dSPM solution.

2.9. Resection and postsurgical outcome

The resection margins were defined based on patient's presurgical evaluation and long-term iEEG monitoring. The goal is to eliminate the SOZ and brain regions that are active during interictal periods. To define the resection volume on patient's MRI, we co-registered the presurgical and postsurgical MRIs using *Brainstorm* (Tadel et al., 2011). We then marked all the volume points, which corresponded to the resection volume, in the co-registered image. A member of the research team (E. Tamilia) who was blind to the marks and results, as well as the patient's outcome defined the resected volume on MRI. Fig. 1d shows the resected volume (green volume in EMSI and ESI-iEEG) overlaid on the preoperative MRI of patient #10. The postsurgical clinical outcome was evaluated using the Engel classification system (Engel, 1993) based on the most recent follow-up of the patient at least 12 months after surgery. The patients were dichotomized into having good (Engel 1) or poor surgical outcome (Engel $\geq$ 2).

2.10. Distance from SOZ and resection

For each ECD source with GOF > 60%, we measured the distance from the clinically defined SOZ (D_{SOZ}) as the Euclidean distance of each ECD source from the nearest SOZ contact and then average (Fig. 1e). Similarly, we estimated the Euclidean distance of each dSPM solution from the closest SOZ contact and then average. Sources with $D_{SOZ} \leq 15$ mm were categorized as concordant to the SOZ, or outside the SOZ otherwise. We also calculated the D_{RES} of each ECD source with GOF > 60%, as their Euclidian distance from the nearest point of the resected volume and then average (Fig. 1f). Similarly, we estimated the Euclidean distance of each dSPM solution from the nearest contact of the resection volume and then average. Sources with a $D_{RES} \leq 15$ mm were categorized as resected.

Table 1
Clinical characteristics of our cohort, including demographics, results of the non-invasive presurgical workup, and invasive recordings with post-surgical outcomes.

Patients' demographics and Clinical Characteristics												
Patient	**Sex**	**Age [y]**	**Outcome (Engel)**	**P/o follow-up [months]**	**^{18}FDG-PET hypo-metabolism areas**	**Ictal SPECT Hyper-perfusion areas**	**Implanted iEEG Electrodes (ECoG+ sEEG)**	**Video EEG**	**Resected Areas**	**Resection of EZ**	**Resection Volume [cm^3]**	**Histology**
1	Male	11	Good (1a)	47	N/A	L iT, aT	88S + 10D	LF, LC	L mF	Complete	8.24	FCD2a
2	Female	7	Good (1a)	26	N/A	LT	90D	L F-C-T	L sT	Complete	13.69	FCD2a
3	Female	14	Poor (3)	31	LT	Interictal: LH	140D	LH, LC	LT	Complete	8.48	FCD (nc)
4	Female	14	Good (1a)	48	LT	L mT	72S	LT	LT	Partial	18.66	FCD2a
5	Female	9	Poor (2a)	70	RP	RP	80S + 20D	R C-P	R C-P	Partial	18.95	FCD1
6	Male	18	Good (1a)	26	L mT, iT	L mT, iT	64S	L aT	L aT	Complete	32.39	FCD3a
7	Male	16	Poor (2b)	25	L mT	RT, LT	88S	LT	LT	Complete	10.9	FCD1a
8	Female	10	Good (1b)	42	LT	LT	112S + 10D	F	R mF	Partial	25.21	FCD2b
9	Female	18	Poor (2a)	32	NL	LF	144S + 10D	NL	LF	Complete	7.38	FCD2b
10	Female	17	Good (1b)	26	L mT	L aT, R aT	72S	L C-P	L P	Complete	8.18	FCD (nc)
11	Male	13	Poor (2)	48	Not done	NL	136S	LT	L F-T	Complete	47.26	FCD3d
12	Male	18	Good (1a)	28	LH	L mT	64S + 30D	L F-C	L F	Complete	21.86	FCD2b
13	Female	12	Good (1a)	29	LF	LF, LT	70D	L F-P	LF	Complete	29.58	FCD2a
14	Male	12	Good (1a)	62	LT	LT	96S	L aT	LT	Complete	4.55	FCD2a
15	Male	18	Poor (3)	25	L iF, pF	L sT, mT	238D	LT	L mT	Complete	30.08	FCD1
16	Male	10	Good (1b)*	12	L F-T	Note done	64S + 60	L C-P	L P-O	Complete	59.97	FCD1
17	Female	10	Poor (3)	53	L F-P	L F-P	96S	LH	L F-P	Partial	10.81	FCD (nc)
18	Female	7	Poor (2a)	51	Not done	RF	72S + 40D	RH	RF	Complete	8.91	FCD2b
19	Male	5	Good (1a)	24	RF	RF pole	128S + 10D	R F-C-P	RF	Complete	74.89	FCD2b
20	Male	18	Good (1a)	33	L LG	Interictal: NL	162D	L F-T	LO	Complete	52.23	FCD2b
21	Female	8	Poor (2)	24	L insula, sT	Interictal: LT	164D	L F-T	LF	Complete	12.42	FCD1
22	Male	15	Good (1a)*	13	R F-P	R aP	102D	RC	RP	Complete	7.64	FCD1
23	Female	17	Good (1a)*	16	LF	LF	72S + 40D	LF	LF	Complete	5.42	FCD2b

The age (y) given is at the time of the invasive long-term recording. N/A = ^{18}FDG-PET was not performed; L = Left; R = Right; T = Temporal; NL = Non Localizing; F = Frontal; C = Central; P = Parietal; T = Temporal; O = Occipital; H = hemisphere; Ins = Insula; N = normal; m = medial; i = inferior; p = Posterior; LG = lingual gyrus; s = superior; a = anterior; l = lateral; nc = FCD histologically confirmed but not further classifiable; S = subdural iEEG electrodes (grids /or strips), D = deep electrodes; FCD = focal cortical dysplasia; ECoG = Electro-corticography; sEEG = Stereo-EEG. * Engel class in this cases was established at the time of the most recent follow which occurred between one and two years after surgery.

2.11. Prediction of surgical outcome

We created receiver operating characteristic (ROC) curves for all three methods ECDs, clustering, and dSPM based on the D_{RES} of each modality. We categorized the localizations as follows: (i) true positives (TP), good outcome patients with complete resection; (ii) true negatives (TN), poor outcome patients with partial resection; (iii) false positives (FP), poor outcome patients with complete resection and (iv) false negatives (FN), good outcome patients with partial resection. The optimum cut-off value that distinguished between low D_{RES} vs. high D_{RES} (complete vs. partial resection) was selected as the ROC curve point indicating the highest value of Youden's index (J), stated as TP/(TP + FN) + TN/(TN + FP) – 1, which measures the overall discriminative power in predicting outcome. In addition, we calculated the positive predictive value [PPV = TP/(TP + FP)], negative predictive value [NPV = TN/(TN + FN)], sensitivity [TP + FN], specificity [TN + FP], and accuracy [TN + TP/(TP + FP + TN + FN] to evaluate the performance of each zone in terms of outcome prediction. We then measured the odds ratio (OR) of becoming seizure free when operation was concordant versus discordant with the localization of the index test: OR = (TP/FP) / (FN/TN).

Finally, we estimated the overlap percentage of ESI and MSI solutions (i.e., ECDs, clustered dipoles, and dSPM) with resection for both good and poor outcome patients. We then estimated the sensitivity, specificity, and accuracy measures derived from the overlap percentage with the resection and postoperative outcomes. We classified the localizations as follows: concordant with resection and seizure-free (TP); concordant with resection and non-seizure-free (FP); discordant with resection and non-seizure-free (TN); and discordant with resection and seizure-free (FN).

2.12. Statistical analysis

To compare IED rates among modalities, we used the Wilcoxon signed-rank test. Mixed effect analysis of variance (ANOVA) was used to compare the D_{SOZ} and D_{RES} among modalities (i.e., ESI, MSI, EMSI, and ESI-iEEG) or source localization methods (i.e., ECD, clustering, and dSPM) with random effects to correct for repeated measurements within patients. Additionally, multiple comparisons analysis was performed with Bonferroni's post-hoc test between all modalities. Furthermore, Wilcoxon signed rank was used to compare the D_{SOZ} and D_{RES} between modalities for each individual patient. For each modality, two-sample t-test was employed to compare D_{SOZ} and D_{RES} between good and poor outcome patients on ECDs, clustering, and dSPM. Binary logistic regression analysis was carried out to test whether D_{RES} was predictive of patient's post-surgical outcome (good vs. poor outcome). Regression analysis was done for ESI, MSI, EMSI and ESI-iEEG modalities using D_{RES}. In addition, binary logistic regression analysis was performed to test whether concordance with resection site was predictive of patient's post-surgical outcome (good vs. poor outcome). Regression analysis was performed for ESI, MSI, EMSI and ESI-iEEG modalities or source localization methods (i.e., ECD, clustering, and dSPM) using concordance with resection site. P-values = 0.05 were considered significant (Stecker et al., 2017). Statistical analysis was performed in MATLAB 2019a (The MathWorks, Inc) and IBM SPSS software.

3. Results

3.1. Patient cohort and resection

Eighty-four patients with FCD associated DRE underwent epilepsy surgery in the selected period. Out of these patients, 23 (12 females, mean age 12.9 ± 4.07; range: 5–18 years) met all inclusion criteria. Six patients showed histopathological features of FCD type I; 12 patients showed FCD type II and two patients had FCD type III. The histology specimens from three patients showed reactive changes and dysplastic features indicative of FCD. The mean follow-up duration was 37 months (range: 12–91 months). Only 33.33% of FCD I patients were seizure free postoperatively (2 of 6) compared to 83.33% of patients with FCD type II (10 of 12). The mean resection volume was measured 22.5 ± 18.5 cm^3 without difference between good and poor outcome patients (21.5 vs. 24 cm^3; p = 0.85). In four cases, the hypothesized EZ was overlapped with the eloquent cortex and/or vascular structures and thus was not completely resected during surgery. Such type of overlap with eloquent cortex and/or vascular structures was not related with outcome (p = 0.65). Each patient's demographics, presurgical clinical localization, iEEG placement, resected region, postsurgical outcome, and follow-up period are shown in Table 1. Fourteen-patients were seizure free (Engel 1); nine-patients were non-seizure free (Engel $\geq$ 2). The iEEG data from most patients have been used in a previous study conducted by our research group (Alhilani et al., 2020).

3.2. IEDs on iEEG, HD-EEG and MEG

We recognized a total number of 5298 IEDs on iEEG across all patients (mean ± standard deviation: 230.34 ± 152.99 IEDs/patient), 1413 IEDs on HD-EEG (61.43 ± 42.63 IEDs/patient), and 2048 IEDs on MEG (89.04 ± 94.18 IEDs/patient). IEDs, which were seen in both MEG and HD-EEG (with a temporal distance of < 30 ms between the two spike peaks) were 1484 (64.52 ± 73.01 IEDs/patient). The mean (±standard deviation) temporal distance between spikes occurred in HD-EEG and MEG signals was 15.02 ± 8.93 ms. Within these spikes, the peak at the HD-EEG signal was preceding the peak at the MEG signal in 62.75% of events. The rate of IEDs recognized on iEEG (29.23 ± 29.91 IEDs/min) was higher than the rates on HD-EEG (5.11 ± 3.55 IEDs/min; p = 0.0017), MEG (7.42 ± 7.84 IEDs/min; p = 0.0021) and the rates on IEDs which were seen in both MEG and HD-EEG at the same time (5.37 ± 6.08 IEDs/min; p = 0.001). A total of 779 ECDs on iEEG (33.86 ± 42.37 ECDs/patient), 812 ECDs on HD-EEG (35.30 ± 22.51 ECDs/patient), 993 ECDs on MEG (43.17 ± 63.30 ECDs/patient), and 984 IEDs on EMSI (42.78 ± 58.99 ECDs/patient) showed a GOF > 60% and were considered for further analysis.

3.3. Distance from SOZ (D_{SOZ})

Differences were observed for the D_{SOZ} (mean ± standard deviation) among modalities [ESI: 29.09 ± 14.07 mm, MSI: 26.40 ± 10.76 mm, EMSI: 24.33 ± 12.26 mm, and ESI-iEEG: 17.03 ± 14.24 mm, p = 0.051; Fig. 2a] for ECDs in patients with good outcome. Similarly, for clustering, differences were seen for the D_{SOZ} among modalities [ESI: 25.04 ± 16.20 mm, MSI: 23.37 ± 8.98 mm, EMSI: 15.18 ± 9.06 mm, and ESI-iEEG: 12.86 ± 14.02 mm, p = 0.039; Fig. 2a] for patients with good outcome. For dSPM, differences were also observed for the D_{SOZ} among modalities [ESI: 24.06 ± 21.68 mm, MSI: 24.03 ± 19.5 mm, EMSI: 22.58 ± 16.03 mm, and ESI-iEEG: 13.63 ± 12.50 mm, p = 0.012; Fig. 2a] in patients with good outcome. EMSI presented shorter D_{SOZ} (15.18 ± 9.06 mm, Fig. 2a) compared to individual modalities [ESI: 25.04 ± 16.20 mm, p = 0.0093; MSI: 23.37 ± 8.98 mm, p = 0.0322] for dipole clustering in patients with good outcome. For patients with good outcome, the D_{SOZ} of EMSI with clustering was comparable to the D_{SOZ} of ESI-iEEG (EMSI: 15.18 ± 9.06 mm, D_{SOZ} for ESI-iEEG: 12.86 ± 14.02 mm, Fig. 2a). No differences were observed among modalities for the poor outcome patients and source localization techniques,

except an increased D_{SOZ} for the EMSI compared to ESI-iEEG (Fig. 2b).

3.4. Distance from resection (D_{RES})

Differences were observed for the D_{RES} (mean ± standard deviation) among modalities [ESI: 23.28 ± 14.73 mm, MSI: 20.56 ± 10.77 mm, EMSI: 14.68 ± 9.02 mm, and ESI-iEEG: 10.35 ± 8.54 mm, p = 0.008; Fig. 2c] for ECDs in patients with good outcome. Similarly, for clustering, differences were observed for the D_{RES} among modalities [ESI: 18.88 ± 17.30 mm, MSI: 15.51 ± 10.11 mm, EMSI: 8.56 ± 6.24 mm, and ESI-iEEG: 3.81 ± 3.95 mm, p = 0.002; Fig. 2c] in patients with good outcome. For the dSPM, differences were detected for the D_{RES} among modalities [ESI: 26.38 ± 17.74 mm, MSI: 23.65 ± 10.57 mm, EMSI: 19.92 ± 10.12 mm, and ESI-iEEG: 6.76 ± 6.59 mm, p = 0.001; Fig. 2c] in patients with good outcome.

EMSI revealed shorter D_{RES} (8.56 ± 6.24 mm; Fig. 2c) compared to individual modalities [ESI: 18.88 ± 17.30 mm, p = 0.039; MSI: 15.51 ± 10.11 mm, p = 0.021] for clustering in patients with good outcome. Similarly, EMSI showed shorter D_{RES} (14.68 ± 9.02 mm; Fig. 2c) compared to individual modalities [ESI: 23.28 ± 14.73 mm, p = 0.013] for ECDs in patients with good outcome. EMSI presented also shorter D_{RES} (19.92 ± 10.12 mm; Fig. 2c) compared to individual modalities [MSI: 23.65 ± 10.57 mm, p = 0.001) for dSPM in patients with good outcome.

For EMSI with ECD, patients with good outcome showed lower D_{RES} (14.68 ± 9.02 mm) compared to patients with poor outcome (29.40 ± 19.16 mm, p = 0.034; Fig. 2c&d). For EMSI with clustering, patients with good outcome revealed lower D_{RES} (8.56 ± 6.24 mm) compared to patients with poor outcome (23.52 ± 14.98 mm, p = 0.022; Fig. 2c&d). For EMSI with dSPM, patients with good outcome revealed lower D_{RES} (19.92 ± 10.12 mm) compared to patients with poor outcome (29.13 ± 10.39 mm, p = 0.031; Fig. 2c&d). Similar differences were observed between patients with good and poor outcomes only for ESI with dSPM, MSI with dSPM, and ESI-iEEG with clustering and dSPM (data not shown).

3.5. Predictive value of interictal activity using D_{RES} with ECDs, clustering, and dSPM

Fig. 3 shows the ROC analysis results for ESI, MSI, and EMSI. ROC analysis revealed an overall higher diagnostic performance (J) for EMSI (70.63%) than ESI (41.27%) and MSI (33.33%) for clustering. ECDs and dSPM showed lower diagnostic performance (J) compared to clustering with ESI, MSI, and EMSI. Similarly, for EMSI, ROC analysis revealed higher AUC (0.81) than ESI (0.70) and MSI (0.61) with clustering (Table 2). ECDs and dSPM showed lower AUC compared to clustering for ESI, MSI, and EMSI (Table 2). Likewise, for EMSI with clustering, ROC analysis displayed higher PPV (86%) than ESI (75%) and MSI (70%) (Table 2). For EMSI with dSPM, ROC analysis revealed lower NPV (63%) than ESI (66%) and MSI (66%) (Table 2). ECDs and clustering showed higher NPV compared to dSPM (Table 2). For the D_{RES} with clustering, regression analysis showed that EMSI (p = 0.02) was able to predict patient's outcome based on its distance from resection, with an OR of 0.86 (CI: 0.75–0.97, Table 2). Individual modalities did not reach significance [ESI: OR of 0.95, CI: 0.89–1.01, p = 0.16; MSI: OR of 0.95, CI: 0.87–1.01, p = 0.13; Table 2]. For EMSI with clustering, regression model analysis showed sensitivity of 92.9% and specificity of 66.7% (p = 0.02; Table 2) respectively. Individual modalities did not reach significance [ESI: sensitivity of 85.7%, specificity of 22.2%, p = 0.16; MSI: sensitivity of 85.7%, specificity of 33.3%, p = 0.13; Table 2]. In addition, for EMSI, regression analysis showed a higher localization accuracy (82.6%) in predicting outcome compared to the individual modalities ESI (60.9%) and MSI (65.2%) for clustering (Table 2). EMSI with clustering achieved localization accuracy (82.6%) comparable to the ESI-iEEG (82.6%, Table 2). ECDs and dSPM showed lower localization accuracy compared to clustering for ESI, MSI, and EMSI (Table 2).

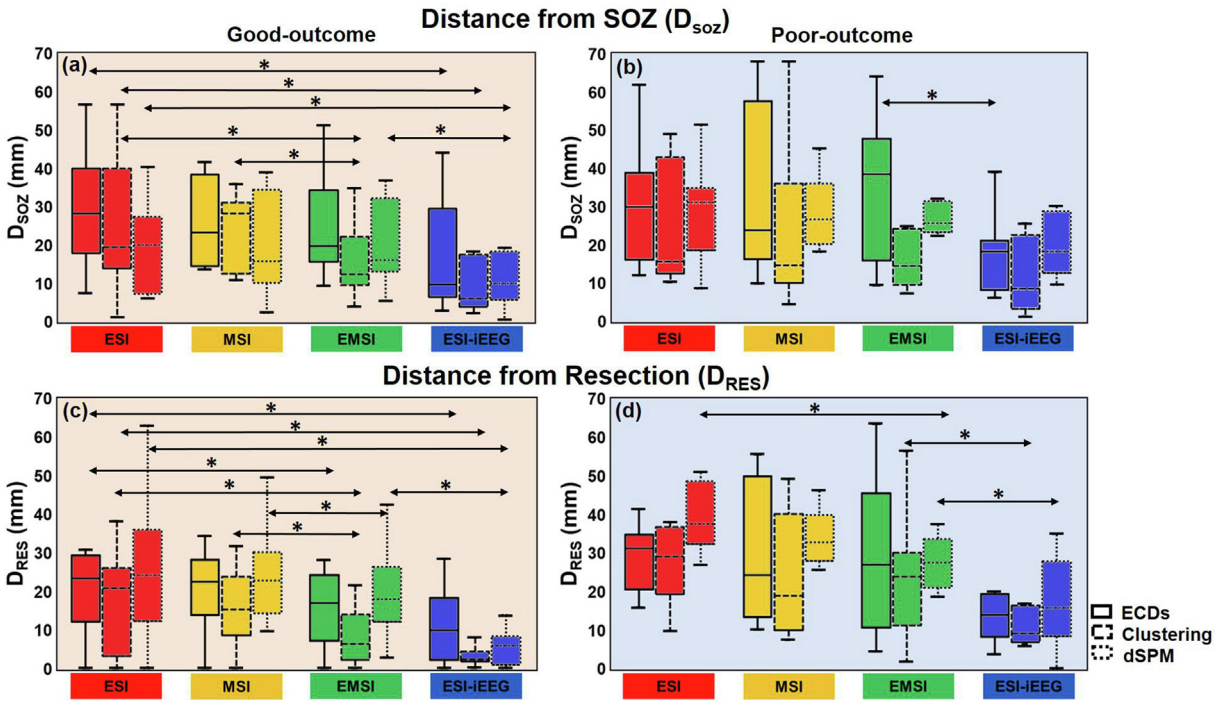

Fig. 2. Estimation of localization accuracy for electric source imaging (ESI), magnetic source imaging (MSI), electromagnetic source imaging (EMSI), and ESI on intracranial EEG (ESI-iEEG). Distance of ECDs, clustered dipoles and dSPM (in mm) from the clinically defined seizure onset zone (SOZ) (D_{SOZ}) for patients with good (a) and poor outcome (b). Distance of ECDs, clustered dipoles and dSPM (in mm) from resection D_{RES} for patients with good (c) and poor outcome (d). Asterisks show significances (p < 0.05).

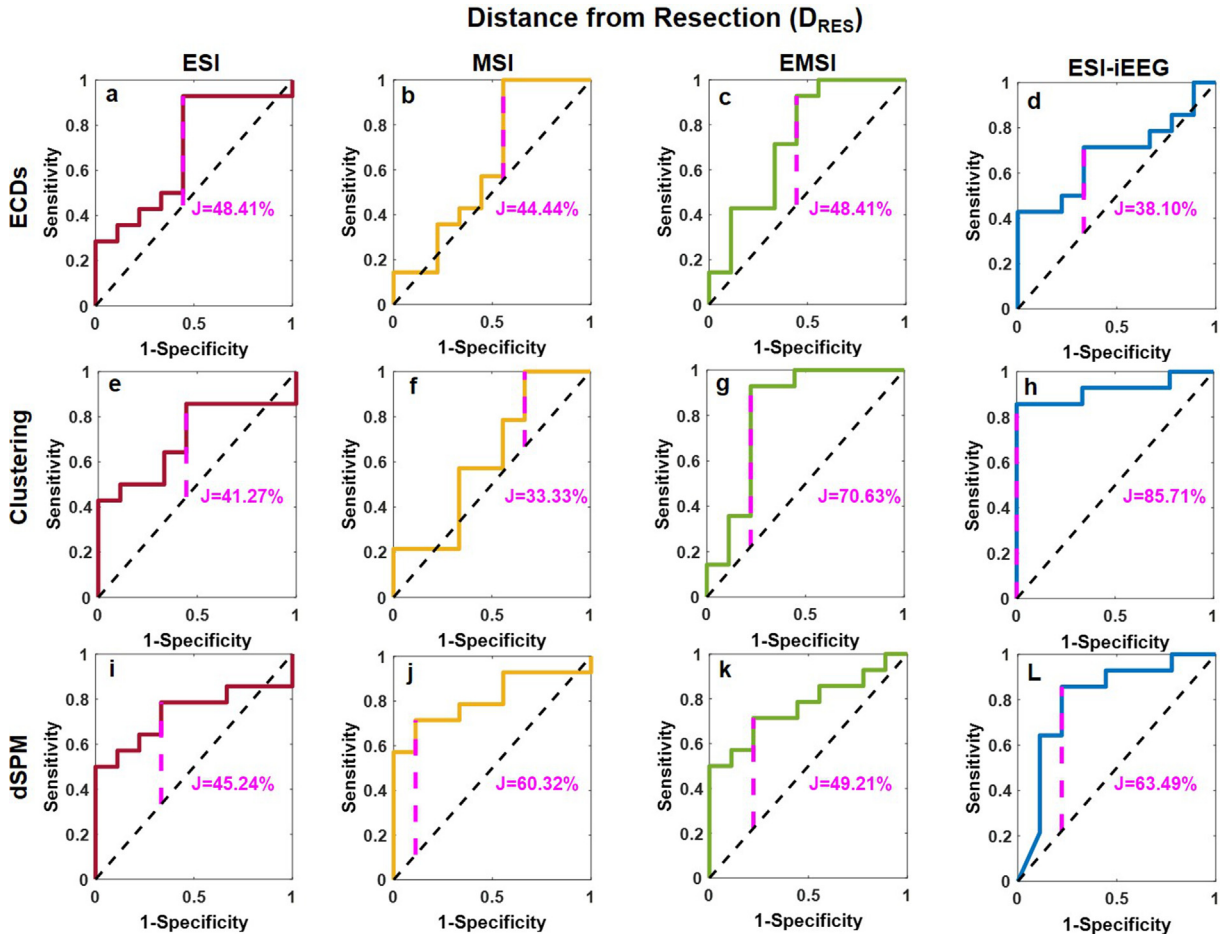

Fig. 3. Predictive surgical outcome for electric source imaging (ESI), magnetic source imaging (MSI), electromagnetic source imaging (EMSI), and ESI on intracranial EEG. Receiver operating characteristic (ROC) curves for predicting surgical outcome for the ESI (a), MSI (b), EMSI (c), and ESI-iEEG (d) with ECDs. ROC curves for predicting surgical outcome for the ESI (e), MSI (f), EMSI (g), and ESI-iEEG (h) with clustering. ROC curves for predicting surgical outcome for the ESI (i), MSI (j), EMSI (k), and ESI-iEEG (l) with dSPM. Dashed vertical lines magenta color mark the Youden's Index (J).

3.6. Predictive value of interictal activity using concordance with resection site

Table 3 presents the performance findings of ESI, MSI, and EMSI for the different source localization techniques (i.e., ECDs, clustering, dSPM) in predicting surgical outcome using as a criterion the concordance with the resection. Regression analysis showed that ESI on iEEG was able to predict surgical outcome for all source localization methods with an OR of 1.13, 1.11, and 1.08, for ECDs, clustering, and dSPM, respectively (Table 3). From the noninvasive source localization methods, EMSI was able to predict outcome for all source localization methods, with an OR of 1.09 (CI: 1.01–1.17; p = 0.018) for ECDs, an OR of 1.33 (CI: 0.97–1.83; p = 0.01) for clustering, and an OR of 1.05 (CI: 1.01–1.09; p = 0.008) for dSPM. Con-

Table 2
Performance of electromagnetic source imaging modalities in presurgical evaluation of FCD patients with distance from resection (D_{RES}) using Binary Logistic Regression Model.

Modalities	Sources	PPV (%)	NPV (%)	AUC	Sensitivity (%)	Specificity (%)	Localization Accuracy (%)	OR (95% CI)	p-value
ESI	**ECDs**	76	83	83	92.9	11.1	60.9	0.96 (0.90–1.03)	0.37
	Clustering	75	71	71	85.7	22.2	60.9	0.95 (0.89–1.01)	0.16
	dSPM	78	66	66	85.7	33.3	65.2	0.94 (0.88–1.00)	0.08
MSI	**ECDs**	73	100	100	85.7	44.4	69.6	0.94 (0.88–1.01)	0.11
	Clustering	70	100	100	85.7	33.3	65.2	0.95 (0.87–1.01)	0.13
	dSPM	90	66	66	78.6	55.6	69.6	0.88 (0.79–0.99)	0.04
EMSI	**ECDs**	76	83	83	92.9	55.6	78.3	0.92 (0.85–1.00)	0.06
	Clustering	86	87	87	92.9	66.7	82.6	0.86 (0.75–0.97)	0.02
	dSPM	83	63	63	85.7	33.3	65.2	0.91 (0.83–1.01)	0.08
ESI-iEEG	**ECDs**	76	60	60	85.7	11.1	56.5	0.94 (0.85–1.03)	0.19
	Clustering	100	81	81	92.9	66.7	82.6	0.70 (0.53–0.93)	0.01
	dSPM	85	77	77	92.9	55.6	78.3	0.88 (0.77–0.99)	0.04

Abbreviations: ESI = Electric Source Imaging; FCD = focal cortical dysplasia; MSI = Magnetic Source Imaging; EMSI = Electromagnetic Source Imaging; ESI-iEEG = Electric Source Imaging performed on intracranial EEG; NPV = Negative Predictive Value; PPV = Positive Predictive Value; Area under Curve (AUC); OR = Odds Ratio; CI = Confidence Interval; p < 0.05.

trarily, individual modalities did not reach significance for any of the source localization methods except for the MSI with dSPM [OR of 1.04, CI: 1.00–1.08, p = 0.03]. EMSI with clustering showed similar localization accuracy (91.3%) with the ESI on iEEG recordings (91.3% for clustering and for dSPM).

3.7. EMSI provides clinically useful information for individual cases

Figs. 4 and 5 show the source localization findings of all modalities for two illustrative cases of patients with FCD-associated DRE having good outcome after surgery (proof of successful delineation and resection of the EZ). In Fig. 4, we present the ESI, MSI, EMSI, and ESI-iEEG source localization findings for a 15 years-old male patient with FCD1. FDG-PET showed an extensive area of hypometabolism covering right frontal and parietal brain regions. Ictal SPECT showed a hyperperfusion in right anterior parietal regions. Video EEG presented with interictal spikes on electrodes covering the right central areas (i.e., electrodes Cz and C4). Retrospective analysis of HD-EEG data with ESI (i.e., ECDs and clustering) showed a tight cluster of dipoles located at the left anterior cingulate cortex (supracallosal gyrus) areas (Fig. 4a). ESI with dSPM showed activity in left caudate nucleus areas (Fig. 4a). MSI with ECDs and clustering showed a tight group of dipoles located in the right inferior frontal gyrus (triangular part) areas (Fig. 4b). MSI with dSPM showed similar activity to ECDs but more middle in right precentral gyrus areas (Fig. 4b). EMSI with all localization techniques (i.e., ECDs, clustering, and dSPM) localized the IEDs closer to resection [ECDs (mean ± standard deviation): 9.63 ± 2.65 mm; clustering: 7.49 ± 0.38 mm; dSPM: 4.73 ± 2.51 mm] compared to ESI (ECDs: 19.45 ± 9.50 mm, p = 0.005; clustering: 15.98 ± 9.53 mm, p = 0.05; dSPM: 14.34 ± 0.62 mm, p = 0.004) and MSI (ECDs: 34.97 ± 4.63 mm, p = 0.01; clustering: 32.31 ± 0.80 mm, p = 0.03; dSPM: 24.89 ± 1.11 mm, p = 0.004) using Wilcoxon rank sum test (Fig. 4c). EMSI with both clustering and dSPM showed overlapping dipoles or activity within the resection (Fig. 4c). ESI on iEEG showed the least-error in localizing the EZ for all three methods (ECDs: 2.55 ± 6.17 mm; clustering: 0.10 ± 0.65 mm; dSPM: 1.64 ± 1.59 mm) and activity within the resection (Fig. 4d).

In Fig. 5, we present the ESI, MSI, EMSI, and ESI-iEEG source localization findings for a 18 years-old male patient with FCD3a. FDG-PET showed an extensive area of hypometabolism covering left medial temporal and inferior temporal brain regions. Ictal SPECT showed a hyperperfusion in left medial temporal and inferior temporal regions. Video EEG presented with IEDs on electrodes covering the left temporal areas (i.e., electrodes T7 and FT9). Retrospective analysis of HD-EEG data with ESI (i.e., ECDs and clustering) showed a tight cluster of dipoles located in the left medial cingulate and paracingulate gyrus areas (Fig. 5a). ESI with dSPM showed activity in left ventral posterolateral nucleus areas (Fig. 5a). MSI with ECDs and clustering showed a tight group of dipoles located in the left medial cingulate and paracingulate gyrus areas (Fig. 5b). MSI with dSPM showed activity in the left anterior cingulate cortex (Fig. 5b). EMSI with all localization techniques (i.e., ECDs, clustering, and dSPM) localized the IEDs closer to resection [ECDs (mean ± standard deviation): 16.77 ± 13.75 mm; clustering: 4.86 ± 0.02 mm; dSPM: 3.04 ± 4.31 mm] compared to the ESI (ECDs: 26.20 ± 11.83 mm, p = 0.02; clustering: 18.18 ± 11.93 mm, p = 0.006; dSPM: 23.96 ± 10.83 mm, p = 0.03) and MSI (ECDs: 26.34 ± 13.86 mm, p = 0.02; clustering: 23.71 ± 14.49 mm, p = 0.01; dSPM: 19.48 ± 2.85 mm, p = 0.004) using Wilcoxon rank sum test (Fig. 5c). EMSI with both clustering and dSPM showed overlapping dipoles or activity within the resection (Fig. 5c). ESI on iEEG showed the least-error in localizing the EZ for all three methods (ECDs: 1.50 ± 2.08 mm; clustering: 0.79 ± 1.78 mm; dSPM: 1.00 ± 1.45 mm) and activity within the resection (Fig. 5d).

4. Discussion

In this study, we evaluated the localization accuracy and diagnostic utility of EMSI in localizing the irritative zone prior to surgery in a cohort of children with FCD-associated DRE. To our best knowledge, very few studies examined so far, the utility of EMSI in pediatric epilepsy (Duez et al., 2019; Abdallah et al., 2022; Pataraia et al., 2005; Neugebauer et al., 2022; Aydin et al., 2014; Sharon et al., 2007), and this study is the first in children with FCD-associated DRE. Localization results obtained by EMSI were superior to those obtained by either modality alone (i.e., ESI or MSI). This result stands for the three different source localization methods we tested: ECDs, clustering, and dSPM. The main results of our study are summarized as follows: (i) EMSI was able to predict surgical outcome for all source localization methods; (ii) EMSI with clustering presented shorter D_{SOZ} and D_{RES} than ESI and MSI alone for good outcome patients who constitute proof of successful localization of the EZ; (iii) EMSI with clustering showed the best localization accuracy compared to ESI and MSI alone; (iv) the D_{SOZ} of EMSI with clustering was comparable to the D_{SOZ} of the ESI performed on iEEG; (v) the Youden's Index (J) was higher for the EMSI (70.63%) than ESI (41.27%) and MSI (33.33%) for clustering; and (vi) ROC analysis revealed higher AUC for EMSI (0.81) than ESI (0.70) and MSI (0.61) alone for the clustering method. Our findings show that EMSI provides improved localization accuracy of the irritative zone compared to individual modalities in children with FCD-associated DRE. Such an accuracy was comparable to invasive modalities (i.e., ESI on iEEG data).

Table 3
Performance of electromagnetic source imaging modalities in presurgical evaluation of FCD patients using concordance with resection zone.

Modalities	Sources	Concordance with Resection (%)	PPV (%)	NPV (%)	Sensitivity (%)	Specificity (%)	Localization Accuracy (%)	OR (95% CI)	p-value
ESI	**ECDs**	32.01	92.3	40	85.7	44.4	69.6	1.06 (0.99–1.13)	0.07
	Clustering	43.18	73.68	100	100	44.4	78.3	1.01 (0.98–1.04)	0.37
	dSPM	28.21	90.9	66.66	71.4	88.9	78.3	1.03 (0.99–1.07)	0.13
MSI	**ECDs**	47.98	70	100	100	33.3	73.9	1.01 (0.97–1.04)	0.56
	Clustering	54.38	70.58	66.66	85.7	44.4	69.6	1.02 (0.99–1.05)	0.15
	dSPM	45.35	73.33	62.5	78.6	55.6	69.6	1.04 (1.00–1.08)	0.03
EMSI	**ECDs**	66.6	84.61	70	78.6	77.8	78.3	1.09 (1.01–1.17)	0.018
	Clustering	80.48	92.85	88.88	92.9	88.9	91.3	1.33 (0.97–1.83)	0.01
	dSPM	61.78	85.71	77.77	85.7	77.8	82.6	1.05(1.01–1.09)	0.008
ESI-iEEG	**ECDs**	74.46	85.71	77.77	77.8	85.7	82.6	1.13 (1.01–1.26)	0.023
	Clustering	84.46	92.85	88.88	92.9	88.9	91.3	1.11 (1.02–1.21)	0.009
	dSPM	71.42	92.85	88.88	92.9	88.9	91.3	1.08 (1.02–1.15)	0.007

Abbreviations: ESI = Electric Source Imaging; FCD = focal cortical dysplasia; MSI = Magnetic Source Imaging; EMSI = Electromagnetic Source Imaging; ESI-iEEG = Electric Source Imaging performed on intracranial EEG; NPV = Negative Predictive Value; PPV = Positive Predictive Value; OR = Odds Ratio; CI = Confidence Interval; $p < 0.05$.

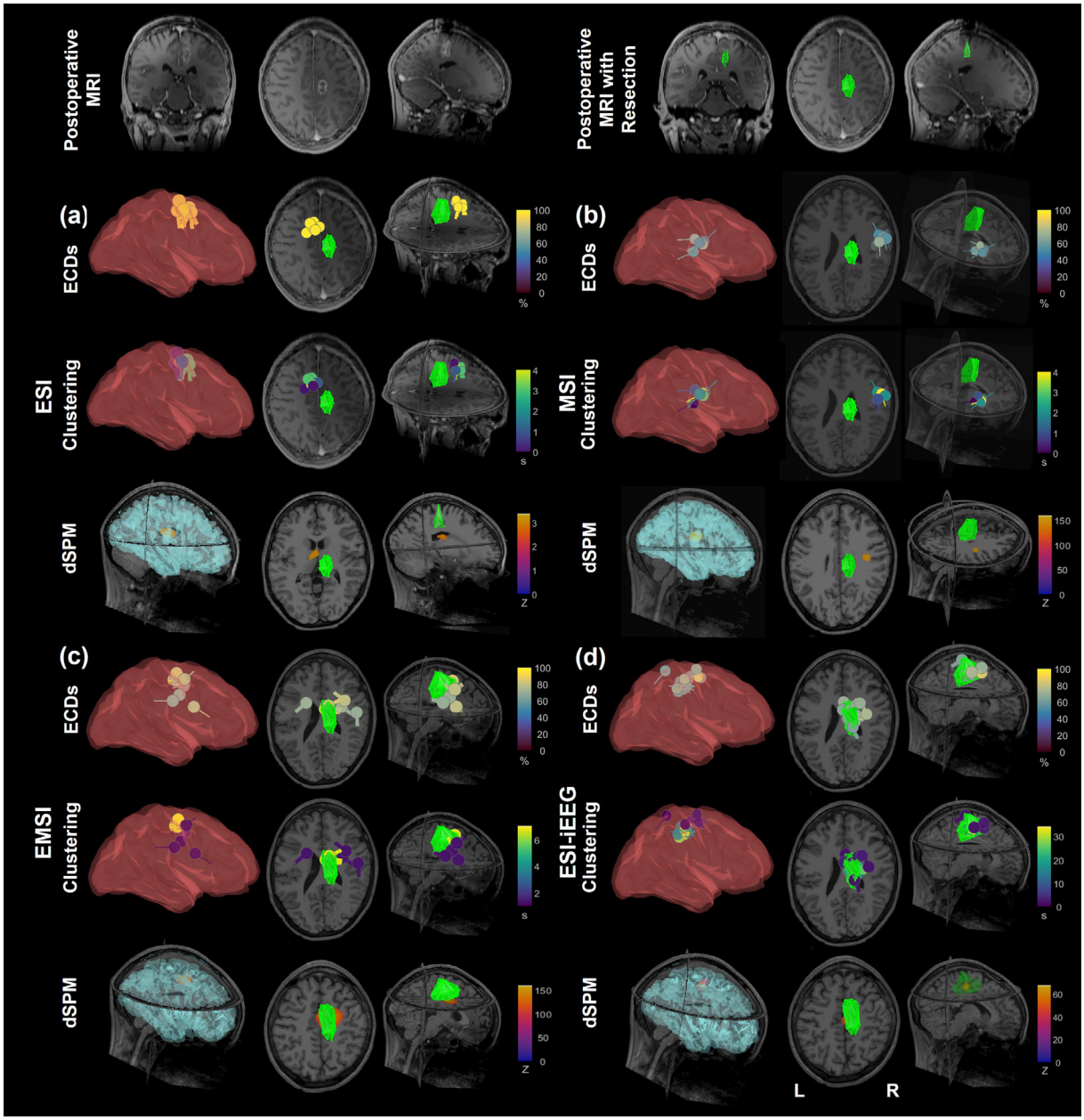

Fig. 4. Example for source localization of all modalities in ESI, MSI, EMSI, and ESI-iEEG for a 15 years-old male patient #22 with FCD1 (good outcome after surgery). The first row shows the postoperative MRI with coronal (left column), sagittal (middle column) and axial (right column) views. ESI (a) with ECDs and clustering showed a tight cluster of dipoles located at the left anterior cingulate cortex (supracallosal gyrus) areas. ESI (a) with dSPM displayed activity in left caudate nucleus areas. MSI (b) with ECDs and clustering showed a tight group of dipoles located in the right inferior frontal gyrus (triangular part) areas. MSI (b) with dSPM presented similar activity to ECDs but more middle in right precentral gyrus areas. EMSI (c) with ECDs, dSPM, and clustering showed overlapping dipoles within the resection (green). Similarly, ESI-iEEG (d) with ECDs, dSPM, and clustering showed overlapping dipoles within the resection (green).

4.1. EMSI is more accurate than ESI and MSI modalities in localizing the irritative zone

Regression analysis showed that EMSI was able to predict outcome for all source localization methods. EMSI with clustering presented the best sensitivity (92.9%), specificity (88.9%), and localization accuracy (91.3%) among all noninvasive source localization methods. EMSI revealed the lowest localization error (D_{SOZ}: ~15 mm; D_{RES}: ~8 mm) compared to individual modalities ESI (D_{SOZ}: ~25 mm; D_{RES}: ~18 mm) and MSI (D_{SOZ}: ~23 mm; D_{RES}: ~15 mm) for clustering in patients with good outcome. EMSI with all techniques localized the irritative zone closer to resection than ESI or MSI modalities not only at the group level but also for individual cases (Figs. 4 & 5). The localization error of ESI and MSI were comparable with former studies in the field. Former studies in patients with DRE undergoing surgery reported that ESI and MSI localized the irritative zone with a localization error of ~ 19 mm for ESI (Birot et al., 2014; Mégevand et al., 2014; Ntolkeras et al., 2022; Tamilia et al., 2019) and ~ 15 mm for MSI (Kim et al., 2016; Ntolkeras et al., 2022; Tamilia et al., 2019). Studies with phantom constructions resembling the electromagnetic properties of human head showed lower localization error of ~ 8 mm for ESI and ~ 3 mm for MSI (Leahy et al., 1998; Papadelis et al., 2009), but they did not consider background noise and co-registration errors due to head movements and other factors affecting the localization accuracy of ESI and MSI.

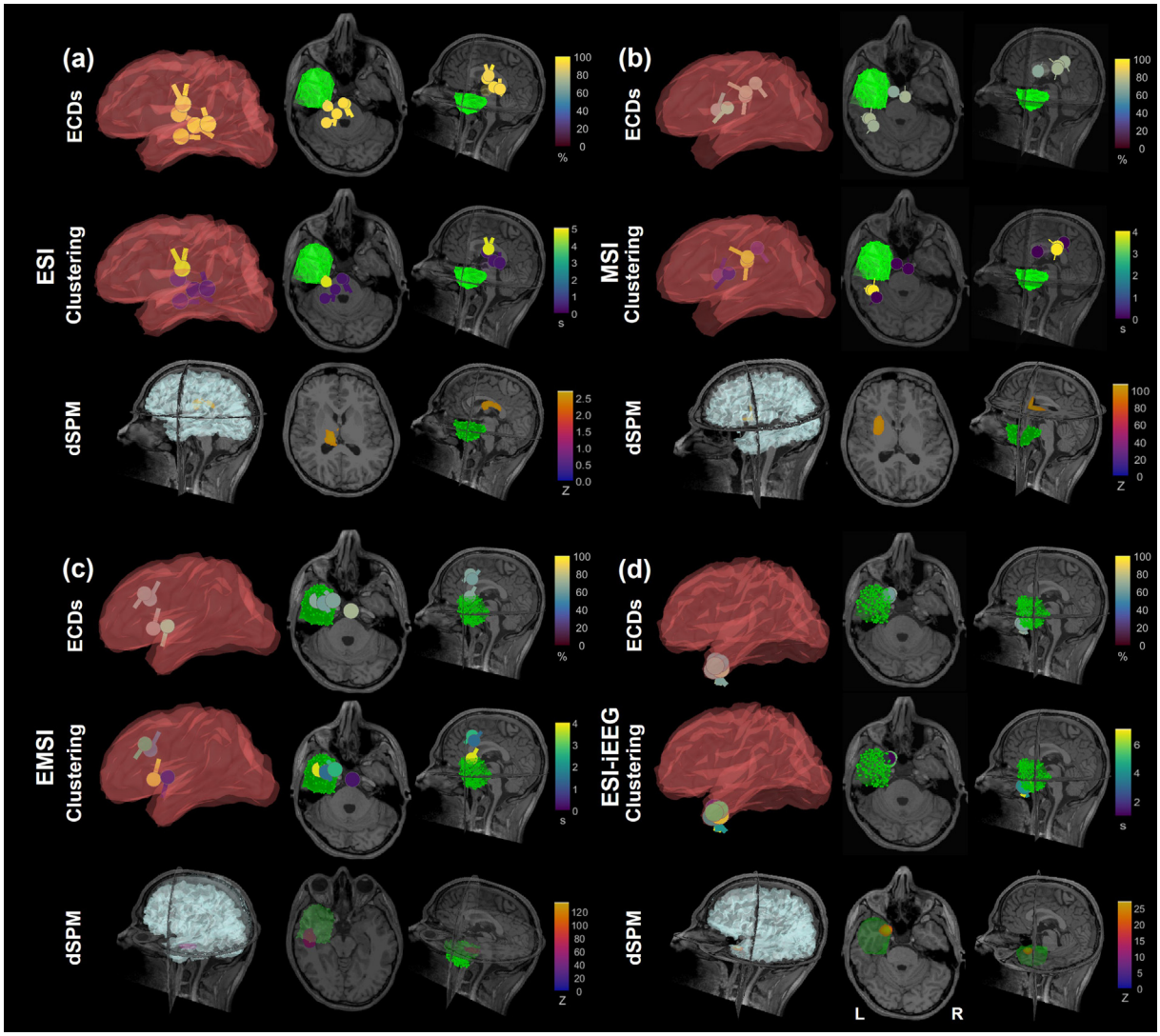

Fig. 5. Example for source localization of all modalities in ESI, MSI, EMSI, and ESI-iEEG for a 18 years-old male patient #6 with FCD3a (good outcome after surgery). ESI (a) with ECDs and clustering showed a tight cluster of dipoles located in the left medial cingulate and paracingulate gyrus areas. ESI (a) with dSPM displayed activity in left ventral posterolateral nucleus areas. MSI (b) with ECDs and clustering revealed a tight group of dipoles located in the left medial cingulate and paracingulate gyrus areas. MSI with dSPM showed activity in the left anterior cingulate cortex. EMSI (c) with ECDs, dSPM and clustering displayed overlapping dipoles within the resection (green). Similarly, ESI-iEEG (d) with ECDs, dSPM, and clustering showed overlapping dipoles within the resection (green).

Here, we obtained the lowest localization error through EMSI with clustering (~8 mm) among all methods performed on noninvasively obtained data. Impressively, this method reached the localization abilities of invasive modalities (i.e., ESI on iEEG data). This is possibly due to the fact that this method combines the advantages of two complementary (in time and space) approaches: (i) clustering that considers the consistency of underlying sources to be localized at the same region in a repetitive manner in time (Ntolkeras et al., 2021); and (ii) EMSI that considers information about the underlying sources from both MEG and HD-EEG, which are complementary in terms of spatial localization abilities (Malmivuo, 2012). The localization of multiple dipoles, which correspond to IEDs occurring at different time points of recordings, within the same gyrus (clustered dipoles) may reflect the existence of a local epileptic neuronal group that can generate epileptiform activity (Kim et al., 2016). EEG and MEG at the scalp reflect in essence similar elementary neuronal phenomena (Lopes da Silva, 2013). EEG records mainly extracellular currents, while MEG is more sensitive to primary intracellular currents (Murakami and Okada, 2006). Thus, EEG and MEG are partially independent modalities. The EEG is sensitive to both tangential and radial components of dipolar sources. On the other hand, the MEG is not sensitive to radial components of dipolar sources but only to the tangential components of a source (Ahlfors et al., 2010). This is because a radially oriented dipolar source does not generate a measurable magnetic field outside a spherical volume conductor. Yet, most previous comparative studies between MSI and ESI showed better localization accuracy for MSI compared to ESI (Ntolkeras et al., 2022; Tamilia et al., 2019) or accuracy of the same order of magnitude (Cohen et al., 1990). Other studies have shown that MEG has higher spatial resolution in separating cortical sources due to less spatial smearing than EEG (Hari, 2011). Hence, recording both MEG and EEG brings some additional information on the bioelectric activity of the brain (Malmivuo, 2012). This can explain the improved localization accuracy of EMSI compared to individual modalities (i.e., ESI or MSI) in our data. Thus, EMSI may offer significant input in estimating the most epileptogenic areas even when the ESI or MSI findings do not help guiding the surgical planning. This can expand the possibility of surgical treatment to patients who would not be otherwise considered surgical candidates.

4.2. Dipole clustering is more accurate than ECDs and dSPM

The concept of dipole clusterness is not new in source localization literature (Paetau et al., 1992; Knowlton et al., 1997; Morioka et al, 1999). A dipole cluster can be defined as a group of multiple ECDs that are closely located together and likely represent a similar neural source in a specific brain area. In general, clustering in ESI or MSI is performed based on the closet IEDs in a small area of the brain, which induced strong neural synchronization (i.e., the combined activity of many neurons firing in a single brain structure) in the brain area (Fischer et al., 2005; Oishi et al., 2006; RamachandranNair et al., 2007). Contrarily, scattered dipoles are distributed within a larger area of the brain (Tamilia et al., 2019), and likely represent multiple neuronal sources in a larger brain area, which may represent a regional epileptogenic network (Corona et al., 2021; 2023; Matarrese et al., 2023). Within this framework, several ESI and MSI studies used dipoles clusters in order to localize the epileptic foci. In most of these studies, the dipole cluster was subjectively detected through visual inspection of dipole distribution maps (Morioka et al., 1999; Fischer et al., 2005; Oishi et al., 2006; RamachandranNair et al., 2007). Other studies used more objective criteria based on the number of dipoles and the spatial contiguity of the spike sources (Iida et al., 2005; Kim et al., 2016; Widjaja et al., 2008; Wilenius et al., 2013). Yet, these criteria are predefined, and their neurophysiological basis is unclear (Tanaka et al., 2018). To overcome these limitations, our group introduced a new definition of dipole clustering that reconsiders the concept beyond the subjective, predefined criteria used in the previous studies (Ntolkeras et al., 2022). By using this algorithm, we showed here that dipole clustering improves the localization accuracy of IEDs compared to ECDs and dSPM for all three investigated modalities (i.e., EMSI, ESI, and MSI). Dipole clustering presented lower D_{RES} (EMSI: ~8 mm; ESI: ~18 mm; MSI: ~15 mm) than ECDs (EMSI: ~14 mm; ESI: ~23 mm; MSI: ~20 mm) and dSPM (EMSI: ~19 mm; ESI: ~26 mm; MSI: ~23 mm) for patients with good outcome, which constitute proof of precise localization of the EZ. Our EMSI findings with dipole clustering showed lower D_{RES} (EMSI: ~8 mm) than previous studies that used the conventional ESI (~15 mm) or MSI (~16 to 19 mm) alone to localize the irritative zone in patients with DRE (Kim et al., 2016; Ntolkeras et al., 2022). Therefore, dipole clustering is a robust source localization approach that can improve the accuracy of EMSI, ESI, and MSI in several clinical scenarios, such as in patients with DRE having normal MRI or FCD.

4.3. EMSI predicts surgical outcome better than ESI or MSI

Few studies assessed the clinical utility of ESI and MSI for patients with FCD-associated DRE reporting a localization accuracy of ~50% for ESI (Bast et al., 2004; Hauptman and Mathern, 2012) and ~45% for MSI (Bast et al., 2004). To our best knowledge, there is no study assessing the clinical utility of EMSI in patients with FCD-associated DRE. In our study, the EMSI predicted surgical outcome better than ESI and MSI alone. The resection of the EMSI presented a higher localization accuracy (~82%, Table 2) with clustering in predicting the patient's outcome than individual modalities alone: ESI (~60%) and MSI (~65%). Similarly, ROC analysis showed an overall higher diagnostic performance for EMSI (J=~70%; Fig. 4g) than ESI (~41%) and MSI (~33%) for clustering. Also, ROC analysis with EMSI revealed higher AUC and odds ratio than ESI and MSI alone. For EMSI with clustering, we found higher sensitivity (~92%; Table 2) than ESI (~85%) and MSI (~85%) alone. EMSI with dipole clustering achieved sensitivity (~92 %) that was comparable to the ESI-iEEG (~92%). It is impressive that a noninvasive source localization method can achieve the localization accuracy and surgical prediction ability of an invasive method. Our findings indicate that EMSI is possibly a valid noninvasive alternative to iEEG, particularly for those patients who are unable to handle invasive investigations, like infants or young children. This supports the line of evidence of a previous prospective EMSI study that showed the presurgical utility of EMSI to potentially replace iEEG in patients with DRE (Duez et al. 2019). The predictive values of ESI and MSI, observed here, are comparable with previous studies in the field (ESI: Kaur et al., 2021; Stefan et al., 2003; Pataraia et al., 2004; Paulini et al., 2007; MSI: Kaur et al., 2021; Stefan et al., 2003; Pataraia et al., 2004; Paulini et al., 2007). Previous studies revealed an ESI sensitivity of ~ 60% and specificity of ~ 47% (Baroumand et al. 2018; Sharma et al., 2018); similarly, MSI revealed a sensitivity of ~ 79% and specificity of ~ 38% (Kaur et al., 2021; Mouthaan et al., 2019; Stefan et al., 2003; Pataraia et al., 2004). In summary, the EMSI seems to provide an improved sensitivity and specificity in the prediction of surgical outcome for patients with FCD-associated DRE compared to individual modalities.

4.4. Limitations

Our study has some limitations. Its retrospective nature may have introduced some biases. For example, although we were able to establish a statistical relationship between the EMSI results and the seizure outcome in retrospect, we were unable to directly assess the effect that the EMSI would have on resection planning and surgical outcome. Moreover, we used a fused EMSI solution that is a simplistic addition of ESI and MSI inverse solutions. More advanced models, which can resemble the complex electromagnetic properties of the human brain, need to be developed, validated and tested (Baillet et al., 1999). Furthermore, HD-EEG and MEG data were simultaneously recorded but not at the same time with iEEG recordings. Thus, IEDs which were recorded with iEEG may differ from the ones recorded with HD-EEG and MEG. Future simultaneous recordings of noninvasive (i.e., HD-EEG and MEG) and invasive data from patients with DRE are thus required. The number of HD-EEG channels (72) and MEG sensors (306) were different between the two modalities. Hence, a direct comparison of the ESI and MSI findings was somehow unfair. Future studies should test comparable number of sensors between the two modalities. Finally, only IEDs which occur in both HD-EEG and MEG recordings were considered for EMSI analysis. Moreover, the EMSI was performed at the mid-point between the spike peaks occurred in the MEG and EEG signals, while the ESI and MSI at the peak of IEDs. It would be interesting to examine in further studies whether the two modalities offer complimentary information when IEDs occur in one but not in the other modality's signal, but also whether localizations at different time-points of IEDs offer better accuracy and surgical prediction values than at other time-points.

5. Conclusion

In this study, we show that EMSI, which fuses information from simultaneous HD-EEG and MEG recordings, provides superior localization accuracy of the epileptogenic focus and improved predictive performance of surgical outcome compared to individual modalities (ESI or MSI) in children with FCD-associated DRE. By combining the EMSI solution with an in-house dipole clustering method, we managed to achieve a localization accuracy that was comparable with the one of invasive methods (iEEG). Our findings indicate that simultaneous HD-EEG and MEG recordings offer critical complimentary and confirmatory information, and EMSI may offer a valid noninvasive alternative to iEEG. This is particularly

important for patients with DRE who cannot handle invasive examinations, such as infants or young children with DRE.

Declaration of competing interest

None of the authors have potential conflicts of interest to disclose.

Acknowledgements

This work was supported by the National Institute of Neurological Disorders & Stroke (RO1NS104116-01A1, PI: C. Papadelis; and R21NS101373-01A1, PIs: C. Papadelis and S. Stufflebeam).

References

Abdallah C, Hedrich T, Koupparis A, Afnan J, Hall JA, Gotman J, et al. Clinical yield of electromagnetic source imaging and hemodynamic responses in epilepsy: validation with intracerebral data. Neurology 2022;98(24):e2499–511.
Ahlfors SP, Han J, Belliveau JW, Hämäläinen MS. Sensitivity of MEG and EEG to source orientation. Brain Topogr 2010;23(3):227–32.
Alhilani M, Tamilia E, Ricci L, Ricci L, Grant PE, Madsen JR, et al. Ictal and interictal source imaging on intracranial EEG predicts epilepsy surgery outcome in children with focal cortical dysplasia. Clin Neurophysiol 2020;131(3):734–43.
Aydin Ü, Vorwerk J, Küpper P, Heers M, Kugel H, Galka A, et al. Combining EEG and MEG for the reconstruction of epileptic activity using a calibrated realistic volume conductor model. PLoS One 2014;9:e93154.
Baillet S, Garnero L, Marin G, Hugonin JP. Combined MEG and EEG source imaging by minimization of mutual information. IEEE Trans Biomed Eng 1999;46:522–34.
Baroumand AG, van Mierlo P, Strobbe G, Pinborg LH, Fabricius M, Rubboli G, et al. Automated EEG source imaging: A retrospective, blinded clinical validation study. Clin Neurophysiol 2018;129(11):2403–10.
Bast T, Oezkan O, Rona S, Stippich C, Seitz A, Rupp A, et al. EEG and MEG source analysis of single and averaged interictal spikes reveals intrinsic epileptogenicity in focal cortical dysplasia. Epilepsia 2004;45:621–31.
Baumgartner C, Pataraia E, Lindinger G, Deecke L. Neuromagnetic recordings in temporal lobe epilepsy. J Clin Neurophysiol 2000;17(2):177–89.
Birot G, Spinelli L, Vulliémoz S, Mégevand P, Brunet D, Seeck M, et al. Head model and electrical source imaging: a study of 38 epileptic patients. Neuroimage Clin 2014;5:77–83.
Blümcke I, Thom M, Aronica E, Armstrong DD, Vinters HV, Palmini A, et al. The clinicopathologic spectrum of focal cortical dysplasias: a consensus classification proposed by an ad hoc Task Force of the ILAE Diagnostic Methods Commission. Epilepsia 2011;52(1):158–74.
Chatrian GE. A glossary of terms most commonly used by clinical electroencephalographers. Electroencephalogr Clin Neurophysiol 1974;37 (5):538–48.
Cohen D, Cuffin BN. A method for combining MEG and EEG to determine the sources. Phys Med Biol 1987;32:85–9.
Cohen D, Cuffin BN. Demonstration of useful differences between magnetoencephalogram and electroencephalogram. Electroencephalogr Clin Neurophysiol 1983;56(1):38–51.
Cohen D, Cuffin BN, Yunokuchi K, Maniewski R, Purcell C, Cosgrove GR, et al. MEG versus EEG localization test using implanted sources in the human brain. Ann Neurol 1990;28(6):811–7.
Corona L, Tamilia E, Madsen JR, Stufflebeam SM, Pearl PL, Papadelis C. Mapping Functional Connectivity of Epileptogenic Networks through Virtual Implantation. Annu Int Conf IEEE Eng Med Biol Soc. 2021;2021:408–11.
Corona L, Tamilia E, Perry MS, Madsen JR, Bolton J, Stone SSD, et al. Non-invasive mapping of epileptogenic networks predicts surgical outcome. Brain 2023;146 (5):1916–31.
Cuffin BN, Cohen D. Comparison of the magnetoencephalogram and electroencephalogram. Electroencephalogr Clin Neurophysiol 1979;47 (2):132–46.
Dale AM, Fischl B, Sereno MI. Cortical surface-based analysis. I. Segmentation and surface reconstruction. Neuroimage 1999;9(2):179–94.
Dale AM, Liu AK, Fischl BR, Buckner RL, Belliveau JW, Lewine JD, et al. Dynamic statistical parametric mapping: combining fMRI and MEG for high-resolution imaging of cortical activity. Neuron 2000;26(1):55–67.
Dallas J, Englot DJ, Naftel RP. Neurosurgical approaches to pediatric epilepsy: indications, techniques, and outcomes of common surgical procedures. Seizure 2020;77:76–85.
De Tiège X, Carrette E, Legros B, Vonck K, Op de Beeck M, Bourguignon M, et al. Clinical added value of magnetic source imaging in the presurgical evaluation of refractory focal epilepsy. J Neurol Neurosurg Psychiatry 2012;83:417–23.
Diekmann V, Becker W, Jürgens R, Grözinger B, Kleiser B, Richter HP, et al. Localisation of epileptic foci with electric, magnetic and combined electromagnetic models. Electroencephalogr Clin Neurophysiol 1998;106 (4):297–313.
Duez L, Tankisi H, Hansen PO, Sidenius P, Sabers A, Pinborg LH, et al. Electromagnetic source imaging in presurgical workup of patients with epilepsy: A prospective study. Neurology 2019;92(6):e576–86.
Engel J Jr. Update on surgical treatment of the epilepsies. In: Summary of the Second International Palm Desert Conference on the Surgical Treatment of the Epilepsies (1992). Neurology. 1993;43(8):1612-1617.
Fischer MJ, Scheler G, Stefan H. Utilization of magnetoencephalography results to obtain favourable outcomes in epilepsy surgery. Brain 2005;128(1):153–7.
Foged MT, Martens T, Pinborg LH, Hamrouni N, Litman M, Rubboli G, et al. Diagnostic added value of electrical source imaging in presurgical evaluation of patients with epilepsy: A prospective study. Clin Neurophysiol 2020;131 (1):324–9.
Fuchs M, Wagner M, Wischmann HA, Köhler T, Theissen A, Drenckhahn R, et al. Improving source reconstructions by combining bioelectric and biomagnetic data. Electroencephalogr Clin Neurophysiol 1998;107:93–111.
Gramfort A, Papadopoulo T, Olivi E, Clerc M. OpenMEEG: opensource software for quasistatic bioelectromagnetics. Biomed Eng Online 2010;9:45.
Hamalainen M, Hari R, Ilmoniemi RJ, Knuutila J, Lounasmaa OV. Magnetoencephalography – theory, instrumentation, and applications to noninvasive studies of the working human brain. Rev Mod Phys 1993;65 (2):413–97.
Hari R. Magnetoencephalography: Methods and Applications. Lippincott Williams & Wilkins; 2011.
Hari R, Puce A. MEG-EEG primer. Oxford University Press; 2017.
Hari R, Baillet S, Barnes G, Burgess R, Forss N, Gross J, et al. IFCN-endorsed practical guidelines for clinical magnetoencephalography (MEG). Clin Neurophysiol 2018;129(8):1720–47.
Hauptman JS, Mathern GW. Surgical treatment of epilepsy associated with cortical dysplasia: 2012 update. Epilepsia 2012;53(Suppl 4):98–104.
Heers M, Rampp S, Kaltenhäuser M, Pauli E, Rauch C, Dölken MT, et al. Detection of epileptic spikes by magnetoencephalography and electroencephalography after sleep deprivation. Seizure 2010;19(7):397–403.
Iida K, Otsubo H, Matsumoto Y, Ochi A, Oishi M, Holowka S, et al. Characterizing magnetic spike sources by using magnetoencephalography-guided neuronavigation in epilepsy surgery in pediatric patients. J Neurosurg 2005;102:187–96.
Kabat J, Król P. Focal cortical dysplasia - review. Pol J Radiol 2012;77(2):35–43.
Kaur K, Garg A, Tripathi M, Chandra SP, Singh G, Viswanathan V, et al. Comparative contribution of magnetoencephalography (MEG) and single-photon emission computed tomography (SPECT) in pre-operative localization for epilepsy surgery: A prospective blinded study. Seizure 2021;86:181–8.
Kim D, Joo EY, Seo DW, Kim MY, Lee YH, Kwon HC, et al. Accuracy of MEG in localizing irritative zone and seizure onset zone: Quantitative comparison between MEG and intracranial EEG. Epilepsy Res 2016;127:291–301.
Knake S, Halgren E, Shiraishi H, Hara K, Hamer HM, Grant PE, et al. The value of multichannel MEG and EEG in the presurgical evaluation of 70 epilepsy patients. Epilepsy Res 2006;69:80–6.
Knight EMP, Gonzalez-Martinez J, Gupta A. Pre-operative evaluation in pediatric patients with cortical dysplasia. Child Nerv Syst. 2015;31:2225–33.
Knowlton RC, Razdan SN, Limdi N, Elgavish RA, Killen J, Blount J, et al. Effect of epilepsy magnetic source imaging on intracranial electrode placement. Ann Neurol 2009;65:716–23.
Knowlton RC, Laxer KD, Aminoff MJ, Roberts TP, Wong ST, Rowley HA. Magnetoencephalography in partial epilepsy: clinical yield and localization accuracy. Ann Neurol 1997;42(4):622–31.
Kwan P, Brodie MJ. Early identification of refractory epilepsy. N Engl J Med 2000;342:314–9.
Leahy RM, Mosher JC, Spencer ME, Huang MX, Lewine JD. A study of dipole localization accuracy for MEG and EEG using a human skull phantom. Electroencephalogr Clin Neurophysiol 1998;107(2):159–73.
Liu AK, Dale AM, Belliveau JW. Monte Carlo simulation studies of EEG and MEG localization accuracy. Hum Brain Mapp 2002;16:47–62.
Lopes da Silva F. EEG and MEG: relevance to neuroscience. Neuron 2013;80 (5):1112–28.
Malmivuo J. Comparison of the properties of EEG and MEG in detecting the electric activity of the brain. Brain Topogr 2012;25(1):1–19.
Matarrese MAG, Loppini A, Fabbri L, Tamilia E, Perry MS, Madsen JR, et al., Papadelis C. Spike propagation mapping reveals effective connectivity and predicts surgical outcome in epilepsy. Brain. 2023 Apr 5:awad118. doi: 10.1093/brain/awad118.
Matarrese MAG, Loppini A, Jahromi S, Tamilia E, Fabbri L, Madsen JR, et al. Electric source imaging on intracranial EEG localizes spatiotemporal propagation of interictal spikes in children with epilepsy. Annu Int Conf IEEE Eng Med Biol Soc. 2021;2021:2668–71.
Morioka T, Nishio S, Ishibashi H, Muraishi M, Hisada K, Shigeto H, Yamamoto T, Fukui M. Intrinsic epileptogenicity of focal cortical dysplasia as revealed by magnetoencephalography and electrocorticography. Epilepsy Res 1999;33(2–3):177–87.
Mouthaan BE, Rados M, Boon P, Carrette E, Diehl B, Jung J, et al. E-PILEPSY consortium. Diagnostic accuracy of interictal source imaging in presurgical epilepsy evaluation: a systematic review from the E-PILEPSY consortium. Clin Neurophysiol 2019;130(5):845–55.
Murakami S, Okada Y. Contributions of principal neocortical neurons to magnetoencephalography and electroencephalography signals. J Physiol 2006;575:925–36.

Neugebauer F, Antonakakis M, Unnwongse K, Parpaley Y, Wellmer J, Rampp S, et al. Validating EEG, MEG and Combined MEG and EEG Beamforming for an Estimation of the Epileptogenic Zone in Focal Cortical Dysplasia. Brain Sci 2022;12(1):114.
Ntolkeras G, Tamilia E, AlHilani M, Bolton J, Ellen Grant P, Prabhu SP, et al. Presurgical accuracy of dipole clustering in MRI-negative pediatric patients with epilepsy: Validation against intracranial EEG and resection. Clin Neurophysiol 2022;141:126–38.
Oishi M, Kameyama S, Masuda H, Tohyama J, Kanazawa O, Sasagawa M, et al. Single and multiple clusters of magnetoencephalographic dipoles in neocortical epilepsy: significance in characterizing the epileptogenic zone. Epilepsia 2006;47(2):355–64.
Ono M, Kubik S, Abernathey CD. Atlas of the cerebral sulci. Stuttgart: Georg Thieme; .
Paetau R, Kajola M, Karhu J, Nousiainen U, Partanen J, Tiihonen J, et al. Magnetoencephalographic localization of epileptic cortex–impact on surgical treatment. Ann Neurol 1992;32(1):106–9.
Papadelis C, Tamilia E, Stufflebeam S, Grant PE, Madsen JR, Pearl PL, et al. Interictal high frequency oscillations detected with simultaneous magnetoencephalography and electroencephalography as biomarker of pediatric epilepsy. J Vis Exp 2016;118:54883.
Papadelis C, Poghosyan V, Fenwick PBC, Ioannides AA. MEG's ability to localise accurately weak transient neural sources. Clin Neurophysiol 2009;120 (11):1958–70.
Pataraia E, Simos PG, Castillo EM, Billingsley RL, Sarkari S, Wheless JW, et al. Does magnetoencephalography add to scalp video-EEG as a diagnostic tool in epilepsy surgery? Neurology 2004;62(6):943–8.
Pataraia E, Lindinger G, Deecke L, Mayer D, Baumgartner C. Combined MEG/EEG analysis of the interictal spike complex in mesial temporal lobe epilepsy. Neuroimage 2005;24(3):607–14.
Paulini A, Fischer M, Rampp S, Scheler G, Hopfengärtner R, Kaltenhäuser M, et al. Lobar localization information in epilepsy patients: MEG–a useful tool in routine presurgical diagnosis. Epilepsy Res 2007;76(2–3):124–30.
Pittau F, Ferri L, Fahoum F, Dubeau F, Gotman J. Contributions of EEG-fMRI to assessing the epileptogenicity of focal cortical dysplasia. Front Comput Neurosc. 2017;11:8.
RamachandranNair R, Otsubo H, Shroff MM, Ochi A, Weiss SK, Rutka JT, et al. MEG predicts outcome following surgery for intractable epilepsy in children with normal or nonfocal MRI findings. Epilepsia 2007;48(1):149–57.
Rosenow F, Lüders H. Presurgical evaluation of epilepsy. Brain 2001;124 (9):1683–700.
Seeber M, Cantonas LM, Hoevels M, Sesia T, Visser-Vandewalle V, Michel CM. Subcortical electrophysiological activity is detectable with high-density EEG source imaging. Nat Commun 2019;10(1):753.
Sharma P, Seeck M, Beniczkey S. Accuracy of interictal and ictal electric and magnetic source imaging: a systematic review and meta-analysis. Front Neurol 2019;10:1250.
Sharma P, Scherg M, Pinborg LH, Fabricius M, Rubboli G, Pedersen B, et al. Ictal and interictal electric source imaging in pre-surgical evaluation: a prospective study. Eur J Neurol 2018;25(9):1154–60.
Sharon D, Hämäläinen MS, Tootell RB, Halgren E, Belliveau JW. The advantage of combining MEG and EEG: comparison to fMRI in focally stimulated visual cortex. Neuroimage 2007;36(4):1225–35.
Singh SP. Magnetoencephalography: Basic principles. Ann Indian Acad Neurol 2014;17(Suppl 1):S107–12.
Stapleton-Kotloski JR, Kotloski RJ, Popli G, Magnetoencephalography GDW. Clin Res Pract Brain Sci 2018;17;8(8):157.;8(8):157.
Stecker M, Pasqualetti P, Barry RJ, Daskalakis ZJ, Siebner HR, Ziemann U. Statistical data analyses for clinical neurophysiology. Clin Neurophysiol 2017;128 (10):1837–8.
Stefan H, Hummel C, Scheler G, Genow A, Druschky K, Tilz C, et al. Magnetic brain source imaging of focal epileptic activity: a synopsis of 455 cases. Brain 2003;126(11):2396–405.
Tadel F, Baillet S, Mosher JC, Pantazis D, Leahy RM. Brainstorm: a user-friendly application for MEG/EEG analysis. Comput Intell Neurosci 2011;2011 879716.
Tadel F, Bock E, Niso G, Mosher JC, Cousineau M, Pantazis D, et al. MEG/EEG Group Analysis With Brainstorm. Front Neurosci 2019;13:76.
Tamilia E, AlHilani M, Tanaka N, Tsuboyama M, Peters JM, Grant PE, et al. Assessing the localization accuracy and clinical utility of electric and magnetic source imaging in children with epilepsy. Clin Neurophysiol 2019;130(4):491–504.
Tamilia E, Dirodi M, Alhilani M, Grant PE, Madsen JR, Stufflebeam SM, et al. Scalp ripples as prognostic biomarkers of epileptogenicity in pediatric surgery. Ann Clin Transl Neurol 2020;7(3):329–42.
Tanaka N, Papadelis C, Tamilia E, Madsen JR, Pearl PL, Stufflebeam SM. Magnetoencephalographic mapping of epileptic spike population using distributed source analysis: comparison with intracranial electroencephalographic spikes. J Clin Neurophysiol 2018;35(4):339–45.
Tassi L, Garbelli R, Colombo N, Bramerio M, Russo GL, Mai R, et al. Electroclinical, MRI and surgical outcomes in 100 epileptic patients with type II FCD. Epileptic Disord 2012;14(3):257–66.
Widjaja E, Otsubo H, Raybaud C, Ochi A, Chan D, Rutka JT, et al. Characteristics of MEG and MRI between Taylor's focal cortical dysplasia (type II) and other cortical dysplasia: surgical outcome after complete resection of MEG spike source and MR lesion in pediatric cortical dysplasia. Epilepsy Res 2008;82(2–3):147–55.
Wilenius J, Medvedovsky M, Gaily E, Metsähonkala L, Mäkelä JP, Paetau A, et al. Interictal MEG reveals focal cortical dysplasias: special focus on patients with no visible MRI lesions. Epilepsy Res 2013;105(3):337–48.
Wolters CH, Anwander A, Tricoche X, Weinstein D, Koch MA, MacLeod RS. Influence of tissue conductivity anisotropy on EEG/MEG field and return current computation in a realistic head model: a simulation and visualization study using high-resolution finite element modeling. Neuroimage 2006;30 (3):813–26.
Wood CC. Application of dipole localization methods to source identification of human evoked potentials. Ann N Y Acad Sci 1982;388:139–55.
Yoshinaga H, Nakahori T, Ohtsuka Y, Oka E, Kitamura Y, Kiriyama H, et al. Benefit of simultaneous recording of EEG and MEG in dipole localization. Epilepsia 2002;43(8):924–8.